Sub-millisecond Translational and Orientational Dynamics of a Freely Moving Single Nanoprobe

Joseph S. Beckwith and Haw Yang[*]

Department of Chemistry, Frick Laboratory, Princeton University, Princeton, New Jersey 08544, United States

E-mail: hawyang@princeton.edu

Abstract

This paper presents a new experiment with which we are able to measure the 3D translational motion of a single particle at $10\,\mu s$ time resolution and with $\sim 10\,nm$ spatial resolution whilst at the same time determining the 3D orientation of the same single particle with $250\,\mu s$ time resolution. These high time resolutions are ~ 40 times greater than previous simultaneous measurements of 3D position and 3D orientation. Detailed numerical simulations and experiments are used to demonstrate that the technique is able to measure 3D orientation at the shot-noise limit. The microscope is also able to simultaneously measure the length or width (with the other assumed) of the plasmonic nanorods used here *in-situ* and non-destructively, which should yield a greater understanding of the underlying dynamics. This technique should be applicable to a broad range of problems where environments which change in space and time may perturb physical and chemical dynamics.

Introduction

Observing 3D translational and orientational motion of single particles in the condensed phase at high time resolution is an outstanding problem in physical chemistry. Orientation is a quantity that can have an intimate impact on reactivity.[1] To give but one example, the electronic coupling parameter which modulates an electron transfer reaction is orientation dependent.[2–4] Orientation can also function as a sensitive reporter on the nanoscale environment, with previous work in bulk[5] and at the single-particle level[6] probing such a quantity. This is relevant in complex systems such as cells, where the local environment can vary strongly with time[7] and position[8]—also potentially affecting chemical dynamics. This can complicate understanding of what are already phenomena that occur on diverse timescales: in the case of proteins the dynamics of protein-ligand interactions, chemical transformations, protein-protein interactions,[9] and protein conformational fluctuations[10] can occur at rates from sub-ms to seconds to minutes.[11] Thus given orientation's relevance to these diverse spatiotemporal dynamics, a technique that is capable of monitoring both 3D orientation and 3D position at a high time (ideally sub-ms) and spatial resolution would be of significant utility. Such a technique should also, ideally, be capable of measuring the 3D position over a large range of particle depths, such as to better understand chemical dynamics in e.g., tissues that can have $\sim$mm size structure.

Multiple techniques have previously been used to determine the 3D orientation, encoded in a polar angle θ and azimuthal angle ϕ, of single particles. Imaging a chromophore[12,13] or a plasmonic nanoparticle's[14] point spread function (PSF) has been shown to encode the orientational information, as has detecting luminescence or scattering induced by multiple different light polarizations. Detection of signals induced by different polarizations has been accomplished for chromophores by cycling excitation polarizations[15–18] and for plasmonic nanoparticles by photothermal[19] or differential interference contrast[20] microscopy. A proposal of a division-of-amplitude polarimeter which required no excitation cycling[21] has also been used in determination of the 3D orientation of chromophores[22,23] and plasmonic nanoparticles.[6] Methods using plasmonic nanoparticles and a specialized camera can reach very high time resolutions, with the highest time resolution we could find being $3.3\,\mu s$.[24] None of the above-mentioned techniques determined the 3D *position* at the same time as the 3D orientation, making them unsuitable for interrogating the spatiotemporal dynamics discussed earlier. Recent PSF engineering experiments[25–27] have determined the 3D orientation and also determined the 3D position to a depth within the Rayleigh range, though combined theoretical and experimental work has improved on such a depth more recently.[28,29] However, these methods both require at the very least 10s of ms per frame, with multiple frames needed for accurate determination of the axial position. What is entirely lacking is a method that can determine the 3D position, at a large depth range, and measure the 3D orientation of a probe at sub-ms time resolutions *simultaneously*.

Here, we describe and characterize a new technique that achieves this. The technique measures the full 3D positional information at high ($10\,\mu s$) time resolution as well as the orientational information of a single particle, also at high ($250\,\mu s$) time resolution. This is accomplished by a new instrument which combines division-of-amplitude polarimetry[21] and real-time 3D single-particle tracking (RT-3DSPT).[30] We further use the division-of-amplitude polarimeter to, at the same time as the position and orientation are determined, perform single-particle dynamic light scattering (SP-DLS)[31] for determination of the shape of gold nanorods (AuNRs). The setup and experimental geometry at the particle are shown in Fig. 1. The use of an AuNR scatterer is what here confers high time resolution to the 3D orientation measurement, due to plasmonic nanoparticles established[32] ability to significantly outperform single fluorophores in terms of photon flux and photostability. Due to the implementation of RT-3DSPT the technique can also determine the position of single particles over a large range of depths—here $15\,\mu m$, but with minor changes to the experimental implementation larger ranges are possible.[33] The technique described here should also be easily implementable for the measurement of the 3D orientation of single emitters as well. This expands

---

[*]To whom correspondence should be addressed

the range of experiments that may characterize the dynamics of 3D translation, 3D orientation and the coupling between these two coordinates in complex systems.
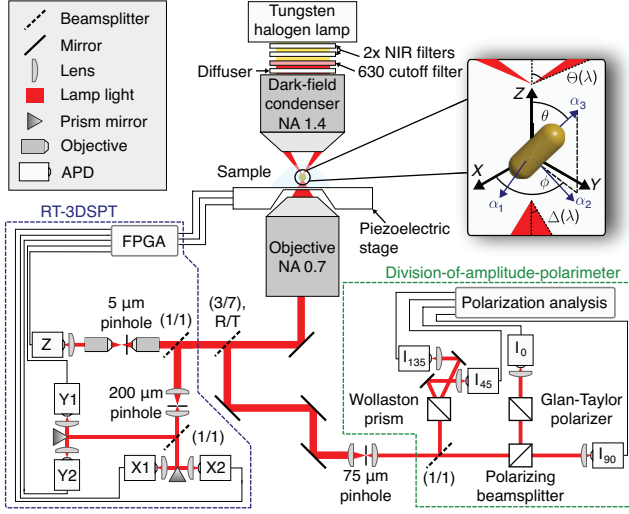
Figure 1: Illustration of the experimental setup. X1, X2, Y1, Y2 and Z represent the APDs used for RT-3DSPT. A non-polarizing beamsplitter, Wollaston Prism and polarizing beam splitter are combined to measure the light polarization of the scattered light at four azimuthal angles—0°, 45°, 90° and 135°. I_0, I_{45}, I_{90} and I_{135} represent the APDs used to measure light at these angles. Zoom-in shows experimental geometry at the particle. Annular light with wavelength λ impinges at an angle $\Theta(\lambda)$, and collected scattered light is bounded by the angle $\Delta(\lambda)$. $\alpha_1(\lambda, S)$, $\alpha_2(\lambda, S)$, and $\alpha_3(\lambda, S)$ are the components of the diagonalized polarizability tensor, and their orientation relative to the axes of the laboratory frame—X, Y, and Z—is described by the angles θ and ϕ. S refers to the particle's shape and volume. The dashed lines indicate the projection of α_3 onto the X–Y plane.

Methods

A schematic of the experimental setup used and the experimental geometry at the particle are shown in Fig. 1. The particle, illuminated with unpolarized light in a dark-field configuration, is freely diffusing but "locked" in the focal volume of the microscope by the RT-3DSPT, such that it is translationally static from the illumination's perspective. We assume that our particles are rod-shaped, and their properties are described by a length l and an width w. These shape parameters, which describe the shape and volume, are indicated by the parameter S. These assumptions allow for a diagonalized polarizability tensor $\boldsymbol{\alpha}$ with S-dependent components $\alpha_1(\lambda, S)$, $\alpha_2(\lambda, S)$, $\alpha_3(\lambda, S)$. Due to the assumed symmetry of the rod, these are related by $\alpha_1 = \alpha_2 \neq \alpha_3$ i.e., $\alpha_{1,2}$ describe the transverse plasmon mode and α_3 the longitudinal. The orientation of these polarizability axes (assumed aligned with the long and short axes of the rod) relative to the laboratory frame is given at time t by the polar angle θ and azimuthal angle ϕ (shown in Fig. 1).

It is important to note that there are three frames of reference that are most relevant here: the laboratory frame (shown by X, Y and Z in Fig. 1), the center-of-mass frame of the particle, and the particle body axis frame (shown by α_1, α_2, α_3 in Fig. 1). A fourth frame relevant to the experiment is that associated with the electric field of the incident or scattered radiation, but a more comprehensive discussion regarding this frame and the transformation between these coordinate systems has been made before.[34] The key point is this: the center-of-mass frame and the lab frame are made coincidental by the use of RT-3DSPT, which in effect performs a *real-time hardware-based mechanical coordinate transform* to do this. As such, this simplifies how we may think about the analysis of the spectroscopic signals arising from this experiment and the dynamics we may uncover with them.

Unlike prolate and oblate spheroids, a simple analytical formula for the jth polarizability tensor element does not exist for rods. Anisotropic nanoparticles are sometimes described using Gans' theory for the electrostatic response of ellipsoids,[35] but here we use the more accurate analytical theory of Yu *et al.*,[36] which uses fits to boundary element method calculations to provide shape-dependent polarizability tensor elements. The relation between these tensor elements to the intensity of the scattered light as a function of 3D orientation has been derived previously,[31,34] we here recapitulate only the essential information for clarity. We detect scattered light at four polarizations, specifically at 0° (*s*-polarized), 45°, 90° (*p*-polarized) and 135° relative to the lab frame. We assume that we illuminate the particle with a series of N discrete wavelengths $\{\lambda\} = \{\lambda_1, \lambda_2, \cdots, \lambda_N\}$ that have corresponding relative intensity weights $\{w\} = \{w_1, w_2, \cdots, w_N\}$. This represents an experimentally measured illumination spectrum and enables us to calculate the expected intensities using lamp illumination, but can also be used to represent a single-wavelength source such as a laser by the simplification of one wavelength and a weight of 1.

Then, the intensity of photons detected at 0°, 45°, 90°, and 135° polarizations are given by

$$I_{s,0,45,90,135°}(t, \{\lambda\}, \{w\}, S) =$$

$$I_0 \Bigg\{ \sum_i^N [W_{11}^{0,45,90,135°} w |\alpha_1|^2] +$$

$$\sum_i^N [W_{13}^{0,45,90,135°} w (\alpha_1 \bar{\alpha}_{3,i} + \bar{\alpha}_1 \alpha_3)]$$

$$+ \sum_i^N [W_{33}^{0,45,90,135°} w |\alpha_3|^2] \Bigg\}. \quad (1)$$

With the wavelength-specific W functions, which relate Θ, Δ, θ and ϕ to specific intensities of particles of shape and volume S described in the supplementary information (Section S1.1). As has been shown by Guerra *et al.*, the initial amplitude of the autocorrelation function A of the polarization contrast fluctuation function

$$\delta\chi(t, \{\lambda\}, \{w\}, S) = \frac{I_{0°} - I_{90°}}{I_{0°} + I_{90°}} - \left\langle \frac{I_{0°} - I_{90°}}{I_{0°} + I_{90°}} \right\rangle$$

is sufficient to fully describe the shape parameter of ellipsoids.[31] Thus we also analyze $A_{\delta\chi}$ in order to determine the length or the width of the AuNR under investigation, though not both (this will be discussed further in the results, Section S4.2).

The implementation of the real-time 3D single particle tracking used in conjunction with the polarization detection has been described before.[30] For completeness, we briefly discuss it here. The technique relies on an active feedback system that uses a 3D piezoelectric stage to compensate for the motion of the tracked particle, locking the particle in the focus of the stationary microscope objective. This is achieved as follows: the scattering from unpolarized, halogen lamp, dark-field illumination is split in a 1:1 ratio, with 50% projected using an optical cantilever of 2 m in length[37] onto two orthogonal prism mirrors. Each prism mirror, one for the

X direction particle motion and the other for the Y particle direction, splits the signal onto two single photon counting avalanche photodiodes (APDs). When a particle is centered in X or Y, the reading on the two corresponding APDs is equal. However, when ~single nm deviations in the particle position occur, the detectors will have an imbalance in their signal that is used for feedback control, with the stage counteracting this motion to return the detectors to balance by moving the particle back to the center of the microscope focus. In this way, the X and Y motion is compensated for, "locking" the particle in the center of the focus in X and Y. To compensate for any motion in the Z (optical axis) direction, 50% of the light sent to the tracking optics was projected through a slightly axially offset pinhole which, when imaged onto an APD, provided a quasi-linear index into the deviation in Z when such an APD intensity is normalized against the four X-Y APDs. The signals from the APDs were used to generate the feedback signals for the piezoelectric stage to keep the particle at the center of the focal volume. This modality of the microscope is shown as the RT-3DSPT box in Fig. 1. The range of the stage used here is $45\,\mu m \times 45\,\mu m \times 15\,\mu m$, which determines the position range over which particles may be tracked. To ensure that there is no interference on the orientational or translational diffusion due to the presence of interfaces,[38,39] particles were tracked starting from the center of the sample chamber, $60\,\mu m$ from the upper and lower chamber surface. More instrumentation details are discussed in the SI, section S2.

When the particle is "locked" in the focal volume of the objective, four APDs were used in the division-of-amplitude polarimeter to measure the intensities at the polarization angles of $0°$, $45°$, $90°$, and $135°$. This was accomplished by the combination of a non-polarizing beamsplitter, Wollaston Prism, and polarizing beamsplitter. The division-of-amplitude polarimeter was characterized using a linear polarizer and a half-wave plate to determine detector balances and polarization extinction ratios, this procedure and these data are shown in Section S3. Further experimental information about sample preparation is found in the SI, section S4. Full detail of the simulator used to describe the experiment is provided in Section S5. Full detail of data analysis for orientation data is provided in Section S6 and tracking data in Section S8.

Results & Discussion

In-situ nanorod length determination

Transmission electron microscopy (TEM) data ($N = 135$) on our AuNR sample are shown in Fig. 2a. Analysis of these data shows that our AuNRs are relatively homogeneous, with an average length of 73.48 nm and an average width of 32.79 nm, corresponding to an average aspect ratio of 2.24. As the SP-DLS monitors only one observable, we cannot simultaneously use the technique to deduce the length *and* width of a single particle, as multiple length-width pairs give the same initial autocorrelation amplitude (shown in Fig. 2b). Thus we use an assumed width from the TEM to get the lengths of our tracked AuNRs from our sample ($N = 399$) in a nominally $c_v = 60\%$ v/v glycerol/water mixture. We note that under these conditions, unlike for prolate ellipsoids,[31] the autocorrelation amplitude does not strictly increase with increasing AuNR length. Thus, it is possible that we assign a shorter rod to being a longer one, or vice versa. This could be corrected by constraining the solutions using the transla-

tional diffusion coefficient from the RT-3DSPT, but we do not do so here. Sizing the AuNRs *in-situ* as they freely diffuse in the 60% v/v glycerol/water mixture gives a length distribution with a similar mean to that found in the TEM, with both means being within one standard deviation of the SP-DLS lengths (Fig. 2c). It not surprising that the means differ, as the SP-DLS technique will "select" AuNRs that have higher scattering coefficients as these provide more tracking signal. Nevertheless, there is remarkable agreement given the inaccurate assumption of a single width in the SP-DLS.
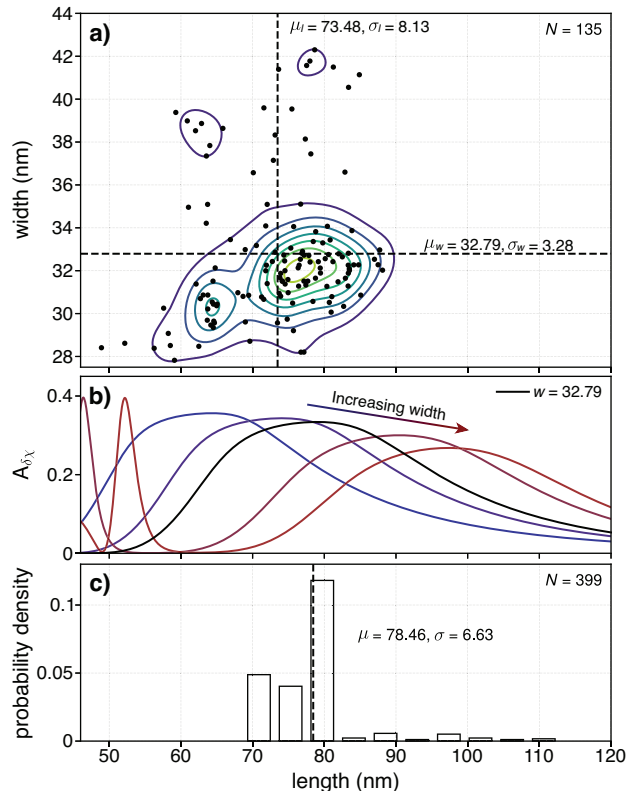

Figure 2: Sizing of AuNRs. a) Length and widths of AuNRs under investigation from TEM, with mean length and width shown. Contours are from kernel density estimation. b) $A_{\delta\chi}$ for a range of lengths and widths, showing that for multiple length-width pairs the $A_{\delta\chi}$ will be the same. From blue to red is increasing width, and the black curve shows the $A_{\delta\chi}$ for a range of lengths at the mean width of the AuNRs from TEM. c) Length data extracted from SP-DLS data assuming the mean width found from TEM.

In addition to giving us better input parameters for the orientational analysis, this enables us to have an estimate as to what diffusion coefficients we anticipate from a freely diffusing AuNR, and thus compare measured dynamics more accurately to a physical model. Importantly we note this is done non-destructively and *in-situ*, meaning spectroscopy can continue to be performed on the same particle after and/or during the sizing. We note that we do have to make an assumption about the width but the effect of a $\pm 10\%$ change on the width is anticipated, based on spherocylinder rotational diffusion equations,[40–42] to have less effect on the observed diffusion coefficients than such a length change. For fully determining the length and width *in situ*, analysis of the single particle scattering spectrum could be related back to the length and width,[43–45] but this goes beyond the scope of this work.

Shot-noise limited measurement uncertainty

To examine the measurement uncertainties in determining 3D orientation using our division-of-amplitude polarimetry technique, we have computed the standard deviation in these aforementioned angle measurements as a function of number of photons used in their determination. In order to do this, we embed AuNRs in a polyacrylamide gel such that they are translationally and rotationally static. As a control to see that the AuNRs are indeed static, we take the autocorrelation functions of each polarization channel and compare to the case of the freely diffusing rods, discussed in the SI, section S7. We also used numerical simulations to benchmark data analysis methods, SI Section S6. Shown in Fig. 3 we compare the standard deviation of the determined θ and ϕ, our measurement uncertainty, with that from the analytical Cramér-Rao lower bounds for this experiment.[46] As we can see, our experimental and analytical technique approaches the shot noise limit. That we approach the shot noise limit is excellent, as it means that our time resolution is simply a function of our specified measurement uncertainty. To put it another way, the only thing necessary for higher time-resolution in orientational dynamics using this experimental modality is more photons. In addition, at a time resolution of 100 photons/time unit, we (for the rod orientation shown here) achieve an uncertainty of ∼11° in θ and ∼7° in ϕ, likely sufficient for many practical applications. It is also of relevance that we have here used a halogen lamp to accomplish this—laser-based dark-field microscopes have been shown to improve photon flux by at least 12 times with respect to lamp illumination,[47] implying a similar improvement in time resolution could be accomplished using a laser. Further improvements in time resolution would likely be possible by optimizing the scatterer used in orientation experiments, though this is also dependent on the illumination source.
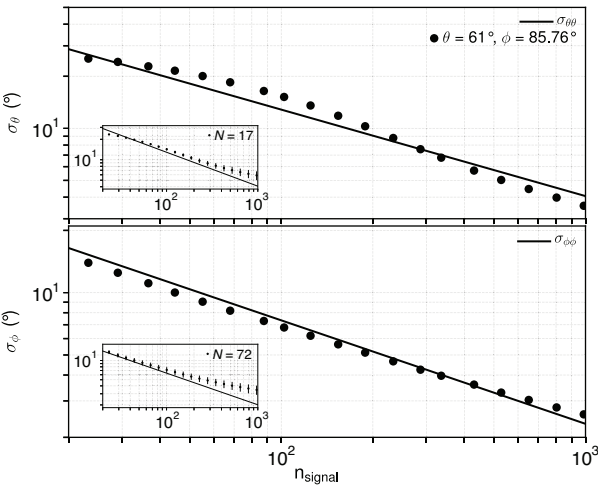
Figure 3: Measurement uncertainty vs Cramér-Rao lower bound. Shown as for a) θ and b) ϕ. Dots are from measurements of a single static rod (orientation annotated) and analytical Cramér-Rao lower bound.[46] Insets show the ensemble average (for θ, orientations of 90° are excluded from the analysis) with error bars showing standard error of the mean.

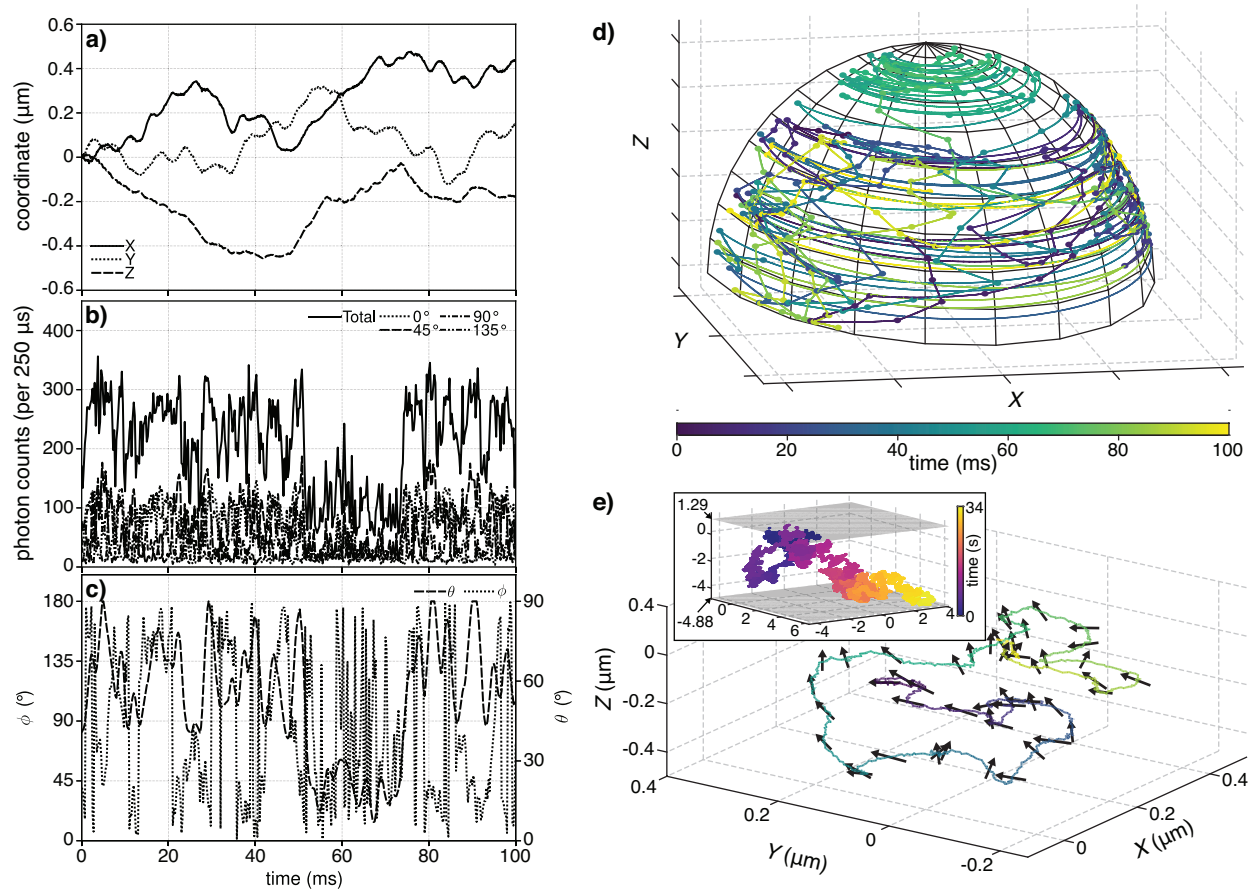## Sub-ms translational and orientational dynamics

With a numerically tested analysis method in hand to determine 3D orientation, and the knowledge that our technique is able to get close to the shot noise limit in analyzing static rods, we analyzed data taken on the freely diffus-

ing AuNRs in order to observe the 3D orientation and 3D position simultaneously as a function of time. Shown in Fig. 4 are results of this analysis for a single AuNR. 100 ms of the translational coordinates of the AuNR are shown in Fig. 4a, showing the rod's diffusion over this time with a D_t of 0.326±0.003 µm²/s. At the same time, we collect photons at the four polarizations discussed earlier, and Fig. 4b shows these photon counts binned to a time resolution of 250 µs. This should give us an approximately 10° measurement uncertainty in θ and 5° measurement uncertainty in ϕ. These photon counts are then, using our analysis algorithm described in the SI, converted into a θ and ϕ at each time point in Fig. 4c. These data are shown as motion on a quarter unit-sphere in Fig. 4d, with the AuNR appearing to explore most of its orientation space within 100 ms. Note well that dipoles exhibit $D_{\infty h}$ rotational symmetry, meaning that we may only uniquely determine their 3D orientation in the range of $0 \le \theta \le 90°$ for θ and $0 \le \phi \le 180°$ for ϕ using this technique. This is in fact the origin of what appear to be large ϕ displacements in the trajectory shown in Fig. 4d, see section S11 of the SI.

Analyzing the entire 34 s track leads to the histograms shown in Fig. S10. These histograms agree reasonably well with what would be expected in the case of free diffusion, though we do see deviations from our expected distributions (marked by dashed lines). Nevertheless, given the number of photons used in each angular determination and the time resolution this affords us, these histograms give further evidence that this technique can determine both the 3D position and 3D orientation as a function of time. Further, these histograms imply that we do not observe significant motional narrowing and/or bias in the angular determination that could arise due to a mismatch between time resolution and the underlying rotational diffusion. Such a phenomenon was discussed recently in experiments mapping the 2D rotational motion of AuNRs on lipid bilayers, where the authors observed significant changes to rotational dynamics by changing time resolution.[48]

The origin of the minor differences between theory and experiment in the ϕ histogram is speculated to be due to temporally- and spatially-varying background noise that is not fully accounted for in our data analysis. For θ, the difference between experiment and theory is likely due[49] to the over-sampling of $\theta = 90°$ as $\theta \to 90°$. It is thus possible that this lamp-based implementation may be somewhat less accurate than laser based approaches, as Molaei *et al.* did not appear to observe this problem,[6] however the approach here gives us information that previously published experiments were not able to access. Most powerfully, we may simultaneously observe 3D orientation and 3D translation at high time resolution. This is shown in Fig. 4e, with the orientation vectors at certain time points shown as the AuNR diffuses in 3D space (not all of the sampled orientations are shown, for clarity of viewing). Thus we have a spectroscopic tool which, for the first time, enables us to simultaneously observe 3D translational and orientational motion at high spatial and sub-ms time resolution. We again reiterate that this high time resolution is, for the 3D orientation, simply dependent on the desired measurement uncertainty and photon flux. Thus, further improvements in time resolution can be anticipated by changing illumination source and/or scatterer. In addition, the new method we present here is able to determine the 3D position over a large axial range of positions, which has presented difficulty for PSF engineering techniques. Indeed, the 15-µm depth-of-field we have here is 3 times the

Figure 4: Analysis and visualization of translational and orientational data. a) 100 ms excerpt of a 34 s track of a single AuNR using the RT-3DSPT module, $D_t = 0.326 \pm 0.003\,\mu m^2/s$, data downsampled to 100 μs time resolution. b) The polarization intensities (photon counts binned to 250 μs) simultaneously recorded for this track. c) The ϕ and θ angles deduced for this 100 ms from the intensities in b). In d) this 100 ms excerpt of orientation is shown mapped to a quarter of a unit sphere, and e) shows the body axis (black arrows) and center-of-mass position in the lab frame for the 100 ms track excerpt. Inset to e) shows the entire 34 s track, with the full 6.36 μm Z-range translation range highlighted.

5-μm depth-of-field that was given by PSF engineering experiments where the explicit goal was to determine 3D position over a wide depth of field.[28] Recent experiments have gone beyond this,[29] giving depths-of-fields comparable to this work, with the additional advantage of being able to track multiple particles in parallel. The advantages of the RT-3DSPT are threefold: there is no need for sophisticated phase masks to be applied to our PSF, the time resolution for 3D tracking is 10 μs, which goes far beyond PSF-engineering methods, and the tracking range is only stage-limited. As with any experiment, the choice of implementation is dependent upon the problem of interest. The inset to Fig. 4e shows the full 34 s track and the 6.36 μm it explores across this time. Using a piezoelectric stage with a larger travel range,[33] even larger axial ranges of particle translation may be explored.

Thus, we are able to simultaneously track, at a time-resolution of 10 μs and at a spatial resolution of ~10 nm in 3D,[37] the 3D position information. Simultaneously, we may determine our 3D orientation at a 250 μs time resolution. This gives us a spectroscopic tool to access the position, orientation, *in-situ* length, translational diffusion coefficients, and rotational diffusion coefficients. Thus, this should in the future enable us to perform analyses of the coupling of these parameters to one another. This therefore has implications for future experiments in complex environments, where local 3D volumes may provide different viscosities which may modulate translational, rotational and possibly chemical dynamics.

Conclusions

We have demonstrated a new instrument that combines RT-3DSPT and a division-of-amplitude polarimeter. With this instrument, we may determine 3D position and 3D orientation at a sub-ms time scale, which previously had not been accomplished experimentally. We have shown that it is possible to simultaneously: track 3D position at a rate of 100 kHz, determine 3D orientation at a rate of 4 kHz, and determine the length of a nanoprobe *in situ*. This instrument is shown to operate close to the shot-noise limit, which means determining the 3D orientation of a nanoparticle at a specified uncertainty is simply a function of photon flux—with further optimization of excitation source and nanoprobe, improvements in time resolution can be expected. A drawback of this instrumentation is that it lacks the high-throughput nature of widefield techniques that are able to measure the 3D position and orientation of many particles at once,[27] though widefield techniques show order-of-magnitudes lower time resolutions than this work. In this light, this work contributes a new tool that experimentalists may use to explore as-yet-unobserved dynamical processes involving orientation. The instrument design described here can also be used, with minor changes, to track luminescent probes (e.g., quantum rods,[22,23,50] which emit at a similar flux to quantum dots and could thus be tracked by the RT-3DSPT technique we show here[51]). It is thus hoped that such an instrument, which provides 3D position and orientation information with unprecedented temporal and spatial resolution, will be of assistance to communities looking into reactions and problems where coupling between 3D space and 3D orientation are relevant. To give a few examples, we may think of virus-membrane interactions[52] in real biological environments,[33] the motion of molecular motors on microtubules[13,23,53] in the cytoskeleton, or imaging heterogeneous polymer matrices, to name but a few. All of these problems are, in their native environments, three-dimensional in nature and thus would benefit from the application of the technique described here. In addition, this technique's unprecedented coupling of 3D spatial and orientational information at high time resolution points to future experiments to probe intra-molecular dynamics, such as electron transfer reactions,[2–4] in heterogeneous systems. This may, in the future, give unprecedented insight into orientation-dependent chemical dynamics in systems that may themselves be spatially and dynamically complex.

Supporting Information Available: W functions for equation 1. Full description of the RT-3DSPT module and the division-of-amplitude polarimeter. Description of characterization of the division-of-amplitude polarimeter. Sample preparation details. Numerical simulation details. Details of data analysis. Details of static rod controls. Translational diffusion coefficients. Rotational diffusion coefficients. Orientation histograms for θ and ϕ. Comparison between measured & simulated ϕ jump data. Description of supplementary videos. The Supporting Information is available free of charge on the ACS Publications website at DOI: 10.1021/acs.jpcb.xxxxxxx. This material is available free of charge via the Internet at http://pubs.acs.org/.

References

(1) Case, D. A.; Herschbach, D. R. Statistical Theory of Angular Distributions and Rotational Orientation in Chemical Reactions. *J. Chem. Phys.* **1976**, *64*, 4212–4222.

(2) Siders, P.; Cave, R. J.; Marcus, R. A. A Model for Orientation Effects in Electron-transfer Reactions. *J. Chem. Phys.* **1984**, *81*, 5613–5624.

(3) Castner, E. W.; Kennedy, D.; Cave, R. J. Solvent as Electron Donor: Donor/Acceptor Electronic Coupling Is a Dynamical Variable. *J. Phys. Chem. A* **2000**, *104*, 2869–2885.

(4) Rumble, C. A.; Vauthey, E. Molecular Dynamics Simulations of Bimolecular Electron Transfer: The Distance-Dependent Electronic Coupling. *J. Phys. Chem. B* **2021**, *125*, 10527–10537.

(5) Sartin, M. M.; Kondo, K.; Yoshizawa, M.; Takeuchi, S.; Tahara, T. Local Environment inside a Novel Aromatic Micelle Investigated by Steady-State and Femtosecond Fluorescence Spectroscopy of an Encapsulated Solvatochromic Probe. *Phys. Chem. Chem. Phys.* **2016**, *19*, 757–765.

(6) Molaei, M.; Atefi, E.; Crocker, J. C. Nanoscale Rheology and Anisotropic Diffusion Using Single Gold Nanorod Probes. *Phys. Rev. Lett.* **2018**, *120*, 118002.

(7) Masuda, T.; Sankowski, R.; Staszewski, O.; Böttcher, C.; Amann, L.; Sagar,; Scheiwe, C.; Nessler, S.; Kunz, P.; van Loo, G. et al. Spatial and Temporal Heterogeneity of Mouse and Human Microglia at Single-Cell Resolution. *Nature* **2019**, *566*, 388–392.

(8) Ebbinghaus, S.; Dhar, A.; McDonald, J. D.; Gruebele, M. Protein Folding Stability and Dynamics Imaged in a Living Cell. *Nat. Methods* **2010**, *7*, 319–323.

(9) Wang, Q.; Moerner, W. E. Single-Molecule Motions Enable Direct Visualization of Biomolecular Interactions in Solution. *Nat. Methods* **2014**, *11*, 555–558.

(10) Yang, H.; Luo, G.; Karnchanaphanurach, P.; Louie, T.-M.; Rech, I.; Cova, S.; Xun, L.; Xie, X. S. Protein Conformational Dynamics Probed by Single-Molecule Electron Transfer. *Science* **2003**, *302*, 262–266.

(11) Chu, J.-W.; Yang, H. Identifying the Structural and Kinetic Elements in Protein Large-Amplitude Conformational Motions. *Int. Rev. Phys. Chem.* **2017**, *36*, 185–227.

(12) Sepioł, J.; Jasny, J.; Keller, J.; Wild, U. P. Single Molecules Observed by Immersion Mirror Objective. The Orientation of Terrylene Molecules via the Direction of Its Transition Dipole Moment. *Chem. Phys. Lett.* **1997**, *273*, 444–448.

(13) Toprak, E.; Enderlein, J.; Syed, S.; McKinney, S. A.; Petschek, R. G.; Ha, T.; Goldman, Y. E.; Selvin, P. R. Defocused Orientation and Position Imaging (DOPI) of Myosin V. *Proc. Natl. Acad. Sci. U.S.A.* **2006**, *103*, 6495–6499.

(14) Xiao, L.; Qiao, Y.; He, Y.; Yeung, E. S. Three Dimensional Orientational Imaging of Nanoparticles with Darkfield Microscopy. *Anal. Chem.* **2010**, *82*, 5268–5274.

(15) Ha, T.; Enderle, T.; Chemla, D. S.; Selvin, P. R.; Weiss, S. Single Molecule Dynamics Studied by Polarization Modulation. *Phys. Rev. Lett.* **1996**, *77*, 3979–3982.

(16) Prummer, M.; Sick, B.; Hecht, B.; Wild, U. P. Three-Dimensional Optical Polarization Tomography of Single Molecules. *J. Chem. Phys.* **2003**, *118*, 9824–9829.

(17) Beausang, J. F.; Schroeder, H. W.; Nelson, P. C.; Goldman, Y. E. Twirling of Actin by Myosins II and V Observed via Polarized TIRF in a Modified Gliding Assay. *Biophys. J.* **2008**, *95*, 5820–5831.

(18) Mehta, S. B.; McQuilken, M.; Riviere, P. J. L.; Occhipinti, P.; Verma, A.; Oldenbourg, R.; Gladfelter, A. S.; Tani, T. Dissection of Molecular Assembly Dynamics by Tracking Orientation and Position of Single Molecules in Live Cells. *Proc. Natl. Acad. Sci. U.S.A.* **2016**, *113*, E6352–E6361.

(19) Chang, W.-S.; Ha, J. W.; Slaughter, L. S.; Link, S. Plasmonic Nanorod Absorbers as Orientation Sensors. *Proc. Natl. Acad. Sci. U.S.A.* **2010**, *107*, 2781–2786.

(20) Xiao, L.; Ha, J. W.; Wei, L.; Wang, G.; Fang, N. Determining the Full Three-Dimensional Orientation of Single Anisotropic Nanoparticles by Differential Interference Contrast Microscopy. *Angew. Chem. Int. Ed.* **2012**, *51*, 7734–7738.

(21) Fourkas, J. T. Rapid Determination of the Three-Dimensional Orientation of Single Molecules. *Opt. Lett.* **2001**, *26*, 211–213.

(22) Ohmachi, M.; Komori, Y.; Iwane, A. H.; Fujii, F.; Jin, T.; Yanagida, T. Fluorescence Microscopy for Simultaneous Observation of 3D Orientation and Movement and Its Application to Quantum Rod-Tagged Myosin V. *Proc. Natl. Acad. Sci. U.S.A.* **2012**, *109*, 5294–5298.

(23) Lippert, L. G.; Dadosh, T.; Hadden, J. A.; Karnawat, V.; Diroll, B. T.; Murray, C. B.; Holzbaur, E. L. F.; Schulten, K.; Reck-Peterson, S. L.; Goldman, Y. E. Angular Measurements of the Dynein Ring Reveal a Stepping Mechanism Dependent on a Flexible Stalk. *Proc. Natl. Acad. Sci. U.S.A.* **2017**, *114*, E4564–E4573.

(24) Enoki, S.; Iino, R.; Niitani, Y.; Minagawa, Y.; Tomishige, M.; Noji, H. High-Speed Angle-Resolved Imaging of a Single Gold Nanorod with Microsecond Temporal Resolution and One-Degree Angle Precision. *Anal. Chem.* **2015**, *87*, 2079–2086.

(25) Backlund, M. P.; Lew, M. D.; Backer, A. S.; Sahl, S. J.; Grover, G.; Agrawal, A.; Piestun, R.; Moerner, W. E. Simultaneous, Accurate Measurement of the 3D Position and Orientation of Single Molecules. *Proc. Natl. Acad. Sci. U.S.A.* **2012**, *109*, 19087–19092.

(26) Curcio, V.; Alemán-Castañeda, L. A.; Brown, T. G.; Brasselet, S.; Alonso, M. A. Birefringent Fourier Filtering for Single Molecule Coordinate and Height Super-Resolution Imaging with Dithering and Orientation. *Nat. Commun.* **2020**, *11*, 5307.

(27) Lu, J.; Mazidi, H.; Ding, T.; Zhang, O.; Lew, M. D. Single-Molecule 3D Orientation Imaging Reveals Nanoscale Compositional Heterogeneity in Lipid Membranes. *Angew. Chem. Int. Ed.* **2020**, *59*, 17572–17579.

(28) Shechtman, Y.; Sahl, S. J.; Backer, A. S.; Moerner, W. E. Optimal Point Spread Function Design for 3D Imaging. *Phys. Rev. Lett.* **2014**, *113*, 133902.

(29) Shechtman, Y.; Weiss, L. E.; Backer, A. S.; Sahl, S. J.; Moerner, W. E. Precise Three-Dimensional Scan-Free Multiple-Particle Tracking over Large Axial Ranges with Tetrapod Point Spread Functions. *Nano Lett.* **2015**, *15*, 4194–4199.

(30) Cang, H.; Xu, C. S.; Montiel, D.; Yang, H. Guiding a Confocal Microscope by Single Fluorescent Nanoparticles. *Opt. Lett.* **2007**, *32*, 2729–2731.

(31) Guerra, L. F.; Muir, T. W.; Yang, H. Single-Particle Dynamic Light Scattering: Shapes of Individual Nanoparticles. *Nano Lett.* **2019**, *19*, 5530–5536.

(32) Yguerabide, J.; Yguerabide, E. E. Light-Scattering Submicroscopic Particles as Highly Fluorescent Analogs and Their Use as Tracer Labels in Clinical and Biological Applications: II. Experimental Characterization. *Anal. Biochem.* **1998**, *262*, 157–176.

(33) Welsher, K.; Yang, H. Multi-Resolution 3D Visualization of the Early Stages of Cellular Uptake of Peptide-Coated Nanoparticles. *Nat. Nanotechnol.* **2014**, *9*, 198–203.

(34) Yang, H. Single-Particle Light Scattering: Imaging and Dynamical Fluctuations in the Polarization and Spectral Response. *J. Phys. Chem. A* **2007**, *111*, 4987–4997.

(35) Link, S.; Mohamed, M. B.; El-Sayed, M. A. Simulation of the Optical Absorption Spectra of Gold Nanorods as a Function of Their Aspect Ratio and the Effect of the Medium Dielectric Constant. *J. Phys. Chem. B* **1999**, *103*, 3073–3077.

(36) Yu, R.; Liz-Marzán, L. M.; de Abajo, F. J. G. Universal Analytical Modeling of Plasmonic Nanoparticles. *Chem. Soc. Rev.* **2017**, *46*, 6710–6724.

(37) Welsher, K.; Yang, H. Imaging the Behavior of Molecules in Biological Systems: Breaking the 3D Speed Barrier with 3D Multi-Resolution Microscopy. *Faraday Discuss.* **2015**, *184*, 359–379.

(38) Lorentz, H. A. A General Theory Concerning the Motion of a Viscous Fluid. *Abhandl. Theor. Phys* **1907**, *1*, 23.

(39) Brenner, H. The Slow Motion of a Sphere through a Viscous Fluid towards a Plane Surface. *Chem. Eng. Sci.* **1961**, *16*, 242–251.

(40) Tirado, M. M.; Martínez, C. L.; de la Torre, J. G. Comparison of Theories for the Translational and Rotational Diffusion Coefficients of Rod-like Macromolecules. Application to Short DNA Fragments. *J. Chem. Phys.* **1984**, *81*, 2047–2052.

(41) Martchenko, I.; Dietsch, H.; Moitzi, C.; Schurtenberger, P. Hydrodynamic Properties of Magnetic Nanoparticles with Tunable Shape Anisotropy: Prediction and Experimental Verification. *J. Phys. Chem. B* **2011**, *115*, 14838–14845.

(42) Wang, A.; Dimiduk, T. G.; Fung, J.; Razavi, S.; Kretzschmar, I.; Chaudhary, K.; Manoharan, V. N. Using the Discrete Dipole Approximation and Holographic Microscopy to Measure Rotational Dynamics of Non-Spherical Colloidal Particles. *J. Quant. Spectrosc. Radiat. Transf.* **2014**, *146*, 499–509.

(43) Lee, K.-S.; El-Sayed, M. A. Dependence of the Enhanced Optical Scattering Efficiency Relative to That of Absorption for Gold Metal Nanorods on Aspect Ratio, Size, End-Cap Shape, and Medium Refractive Index. *J. Phys. Chem. B* **2005**, *109*, 20331–20338.

(44) Becker, J.; Schubert, O.; Sönnichsen, C. Gold Nanoparticle Growth Monitored in Situ Using a Novel Fast Optical Single-Particle Spectroscopy Method. *Nano Lett.* **2007**, *7*, 1664–1669.

(45) Muskens, O. L.; Bachelier, G.; Fatti, N. D.; Vallée, F.; Brioude, A.; Jiang, X.; Pileni, M.-P. Quantitative Absorption Spectroscopy of a Single Gold Nanorod. *J. Phys. Chem. C* **2008**, *112*, 8917–8921.

(46) Beckwith, J. S.; Yang, H. Information Bounds in Determining the 3D Orientation of a Single Emitter or Scatterer Using Point-Detector-Based Division-of-Amplitude Polarimetry. *J. Chem. Phys.* **2021**, *155*, 144110.

(47) Noda, N.; Kamimura, S. A New Microscope Optics for Laser Dark-Field Illumination Applied to High Precision Two Dimensional Measurement of Specimen Displacement. *Rev. Sci. Instrum.* **2008**, *79*, 023704.

(48) Mazaheri, M.; Ehrig, J.; Shkarin, A.; Zaburdaev, V.; Sandoghdar, V. Ultrahigh-Speed Imaging of Rotational Diffusion on a Lipid Bilayer. *Nano Lett.* **2020**, *20*, 7213–7219.

(49) Lu, C.-Y.; Vanden Bout, D. A. Analysis of Orientational Dynamics of Single Fluorophore Trajectories from Three-Angle Polarization Experiments. *J. Chem. Phys.* **2008**, *128*, 244501.

(50) Hu, J.; Li, L.-s.; Yang, W.; Manna, L.; Wang, L.-w.; Alivisatos, A. P. Linearly Polarized Emission from Colloidal Semiconductor Quantum Rods. *Science* **2001**, *292*, 2060–2063.

(51) Zhao, T.; Beckwith, J. S.; Amin, M. J.; Pálmai, M.; Snee, P. T.; Tien, M.; Yang, H. Leveraging Lifetime Information to Perform Real-Time 3D Single-Particle Tracking in Noisy Environments. *J. Chem. Phys.* **2021**, *155*, 164201.

(52) Kukura, P.; Ewers, H.; Müller, C.; Renn, A.; Helenius, A.; Sandoghdar, V. High-Speed Nanoscopic Tracking of the Position and Orientation of a Single Virus. *Nat. Methods* **2009**, *6*, 923–927.

(53) Forkey, J. N.; Quinlan, M. E.; Alexander Shaw, M.; Corrie, J. E. T.; Goldman, Y. E. Three-Dimensional Structural Dynamics of Myosin V by Single-Molecule Fluorescence Polarization. *Nature* **2003**, *422*, 399–404.

Graphical TOC Entry

Tungsten halogen lamp

Dark-field condenser

Objective

Sub-ms tracking of 3D orientation and 3D translation